Effects of positive-ion resonances in photoionization of neutral atoms

S. L. Haan, M. Bolt, and H. Nymeyer
Department of Physics and Astronomy, Calvin College, Grand Rapids, Michigan 49546

R. Grobe
Department of Physics and Astronomy, University of Rochester, Rochester, New York 14627
(Received 8 December 1994)

Single photoionization of neutral atoms is examined theoretically for a situation in which the photoionizing laser is tuned close to the resonant frequency for transitions between the ground and first-excited states of the positive ion. The resonant coupling in the positive ion is shown to have a dramatic peak-splitting effect on the kinetic-energy spectrum of the ionized electron. An essential-states analysis of the photoionization process is presented, and a comparison is made with numerical results for one-dimensional helium. The agreement between the results establishes the validity of the essential-states approach. The possibility of superposing this core-coherence effect with laser-induced autoionization effects is considered.

PACS number(s): 32.80.Fb, 32.80.Dz, 32.80.Rm

I. INTRODUCTION

It is well known that laser-induced coherences within photoionizing or photodetaching systems can influence the energy spectrum of the ejected electrons. For example, tuning a laser to drive transitions between the initial atomic state and an excited discrete state can lead to Rabi oscillations within the ionizing atom and an ac-Stark shifting of the atomic states. This shifting can then be manifest in the photoelectron spectrum as what is often called the Knight doublet [1,2]. The formation of the doublet can also be described by introducing new dressed states which partially incorporate effects of the external field. Formally, projection operators [3] can be employed to partition the relevant state space into discrete-state and continuum subspaces. A diagonalization of a finite sector of the discrete-state space (in the rotating-wave approximation) gives the dressed atomic states, and inclusion of coupling to the space of continuum states then leads to "decaying dressed states."

Other photoionization processes, such as above-threshold ionization [4], can be described by dressing the continuum states [5] rather than the discrete states of the system. Also, in two-laser Λ configurations, a chosen decay continuum can be structured or dressed by a laser that couples the continuum to a chosen unpopulated discrete state [6].

Laser-induced coherences in photoionizing or photodetaching systems traditionally involved only a single electron, but can also involve two or more electrons. For example, tuning a laser to an autoionizing resonance can lead to Rabi oscillations involving the autoionizing state and to a superposing of ac-Stark effects with two-electron phenomena such as Fano resonances [7–9]. Laser-induced autoionization effects (LIA) have been extensively studied.

Two recent works [10,11] have predicted a new coherence phenomenon that is explicitly a two-electron effect. Reference [10] considers photodetachment of a negative ion, and predicts that one can produce a doublet in the photoelectron spectrum by tuning the detaching laser to a resonant frequency of the neutral atom. The results are explained in terms of a "coherence transfer" from the inner electron of the negative ion, which is resonantly driven between states of the neutral atom, to the outer, photodetaching electron. Reference [11] considers photoionization of neutral atoms, and explores extensions of the coherence transfer theme in that context. It predicts the formation of a doublet in the photoelectron spectrum if the ionizing laser is tuned to an appropriate resonant frequency of the positive ion. Reference [11] also suggests superposing coherence-transfer effects with the effects of laser-induced autoionization. Both Refs. [10] and [11] compare results of essential-states calculations with full numerical results that were obtained by integrating the time-dependent Schrödinger equation, and the works establish the appropriateness of essential-states analysis of such systems.

In the present work, we present details of the essential-states study that was introduced in Ref. [11], and we carefully consider how coherence-transfer and laser-induced autoionization effects can be superposed. We also compare the predictions of the essential-states model with full numerical results for one-dimensional helium, a model two-electron system in which charged particles interact via a screened Coulomb potential [12–14].

The essential-states description we present is general and can be applied either to model systems or to real atoms by choosing appropriate energies and couplings for the various states. In the present work, we use one-dimensional helium as a testing ground for the essential-states analysis because it allows us to compare predictions of the essential-states model with an exact numerical solution of the time-dependent Schrödinger equation.

We consider specifically the essential-states system il-

lustrated in Fig. 1, and consisting of a ground state $|g\rangle$, first excited state $|b\rangle$, autoionizing state $|a\rangle$, and two continua $\{|1,E_k\rangle\}$ and $\{|2,E_k\rangle\}$. The continuum-energy variable E_k denotes the asymptotic kinetic energy of the unbound electron, so the total energy of the continuum state $|j,E_k\rangle$ is the sum E_j+E_k, where E_j is the energy of state $|j\rangle$ of the positive ion. The autoionizing state is coupled to $\{|1,E_k\rangle\}$ by configuration interaction. The other couplings that are shown arise from a laser of frequency ω. In order to concentrate on the core-coherence effect, we choose $|b\rangle$ as our initial state.

If there were no electron-electron interaction, then the states would be simple product states, with the ground state corresponding to $|1,1\rangle$ (or $|1\rangle\otimes|1\rangle$), $|b\rangle$ to $|1,2\rangle$, and $|a\rangle$ to $|2,2\rangle$. In this case the energy difference between the states $|1,1\rangle$ and $|1,2\rangle$ would be the same as between transition $|1,2\rangle$ and $|2,2\rangle$, and both would be the same as the energy difference between $|1\rangle$ and $|2\rangle$ in the positive ion. Of course, the electron-electron interaction prevents the states from being product states and shifts the various states differently, so that the transition frequencies will, in general, no longer be equal. We, therefore, allow for unequal energy separations in our model. Nonetheless, the transition frequencies when the electron-electron interaction is included can still be similar enough that all the states and transitions indicated in Fig. 1 could be relevant for describing the time development of a real atomic system in an external laser field.

In Sec. II, we present the Laplace transform formalism for solving the essential-states model of Fig. 1 for a system initially in state $|b\rangle$. In Sec. III, we analyze the long-time kinetic-energy spectra for various simplified cases. We look first at the situation in which there is no direct photoabsorption from the autoionizing state $|a\rangle$ (i.e., $V_{a,2E}=0$), but then move on to consider the effects of photoabsorption from $|a\rangle$. We conclude Sec. III with a dressed-continuum explanation of our results. In Sec. IV, we return to our full essential-states solution and we compare its predictions with exact numerical results for one-dimensional helium. Finally, in Sec. V, we summarize our results and discuss the coherence effect more fully.

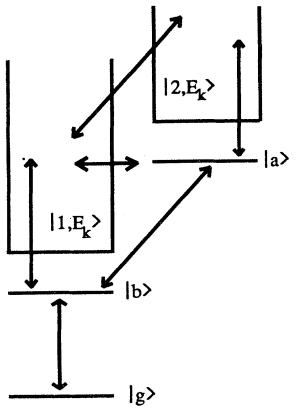

FIG. 1. Schematic of atomic states and couplings included in the analysis.

II. FORMAL SOLUTION

In setting up the essential states problem, we make the rotating-wave approximation and write $H=H^0+W(t)$ where

$$H^0=|g\rangle E_g\langle g|+|b\rangle E_b\langle b|+|a\rangle E_a\langle a|+\int_0^\infty|1,E_k\rangle(E_1+E_k)\langle 1,E_k|dE_k+\int_0^\infty|2,E_k\rangle(E_2+E_k)\langle 2,E_k|dE_k\ ,$$

$$W(t)=\left\{|g\rangle V_{gb}e^{i\omega t}\langle b|+|b\rangle V_{ba}e^{i\omega t}\langle a|+\int_0^\infty|b\rangle V_{b,1E}e^{i\omega t}\langle 1,E_k|dE_k+\int_0^\infty|a\rangle V_{a,1E}\langle 1,E_k|dE_k\right.$$
$$\left.+\int_0^\infty|a\rangle V_{a,2E}e^{i\omega t}\langle 2,E_k|dE_k+\int_0^\infty\int_0^\infty[|1,E_k\rangle\langle 1E_k|H|2E_k'\rangle\langle 2,E_k'|]dE_k dE_k'\right\}+\text{H.c.} \tag{1}$$

Throughout this work we assume all the $V_{\alpha\beta}$ real. For the continuum-continuum coupling we adopt the δ-function coupling ansatz of Refs. [10] and [11],

$$\langle 1E_k|H|2E_k'\rangle=V_{12}e^{i\omega t}\delta(E_k-E_k')\ . \tag{2}$$

This coupling conserves the kinetic energy of the unbound electron and can be thought of as a transition involving only the "core" or nonionized electron. The appropriateness of using this coupling for the situation of interest in this manuscript has been established in Refs. [10] and [11], and will be further established in Sec. IV.

We write the time-dependent state vector in the interaction picture

$$|\psi(t)\rangle=|a\rangle c_a(t)e^{-iE_a t}+|b\rangle c_b(t)e^{-iE_b t}+|g\rangle c_g(t)e^{-iE_g t}+\int_0^\infty|1,E_k\rangle c_1(E_k,t)e^{-i(E_1+E_k)t}dE_k$$
$$+\int_0^\infty|2,E_k\rangle c_2(E_k,t)e^{-i(E_2+E_k)t}dE_k\ . \tag{3}$$

The time-dependent Schrödinger equation then yields the coupled differential equations,

$$
\begin{aligned}
i\dot{c}_1(E_k,t) &= V_{12}c_2(E_k,t)e^{i\Delta t} + V_{1E,a}c_a(t)e^{i(E_k+E_1-E_a)t} \\
&\quad + V_{b,1E}c_b(t)e^{i(E_1+E_k-E_b-\omega)t} , \\
i\dot{c}_2(E_k,t) &= V_{21}c_1(E_k,t)e^{-i\Delta t} + V_{2E,a}c_a(t)e^{i(E_2+E_k-E_a-\omega)t} , \\
i\dot{c}_a(t) &= V_{ab}c_b(t)e^{i(E_a-E_b-\omega)t} \\
&\quad + \int_0^\infty V_{a,1E}c_1(E_k,t)e^{i(E_a-E_1-E_k)t}dE_k \\
&\quad + \int_0^\infty V_{a,2E}c_2(E_k,t)e^{i(E_a+\omega-E_2-E_k)t}dE_k , \\
i\dot{c}_b(t) &= V_{bg}c_g(t)e^{i(E_b-E_g-\omega)t} + V_{ba}c_a(t)e^{i(E_b+\omega-E_a)t} \\
&\quad + \int_0^\infty V_{b,1E}c_1(E_k,t)e^{i(E_b+\omega-E_1-E_k)t}dE_k , \\
i\dot{c}_g(t) &= V_{gb}c_b(t)e^{i(E_g+\omega-E_b)t} ,
\end{aligned}
\tag{4}
$$

where

$$
\Delta = E_1+\omega-E_2 , \tag{5}
$$

represents the detuning from the core ($|1\rangle \leftrightarrow |2\rangle$) resonance of the positive ion.

To begin our solution, we take the Laplace transforms of these equations for the initial condition $c_b(0)=1$, assuming instantaneous turn on of the interaction W. The resulting equations can be written using energy differences

$$
\begin{aligned}
\Delta_E &= E_k+E_1-E_a , \\
\Delta_{ga} &= E_g+2\omega-E_a , \\
\Delta_{ba} &= E_b+\omega-E_a ,
\end{aligned}
\tag{6}
$$

as

$$
\begin{aligned}
(is-\Delta_E)\hat{c}_1(E_k,s+i\Delta_E) &= V_{12}\hat{c}_2[E_k,s+i(\Delta_E-\Delta)] \\
&\quad + V_{1E,a}\hat{c}_a(s) \\
&\quad + V_{1E,b}\hat{c}_b(s+i\Delta_{ba}) , \\
[is-(\Delta_E-\Delta)]\hat{c}_2[E_k,s+i(\Delta_E-\Delta)] &= V_{21}\hat{c}_1(E_k,s+i\Delta_E)+V_{2E,a}\hat{c}_a(s) , \\
is\hat{c}_a(s) &= V_{ab}\hat{c}_b(s+i\Delta_{ba}) \\
&\quad + \int_0^\infty dE_k\{V_{a,1E}\hat{c}_1(E_k,s+i\Delta_E) \\
&\quad + V_{a,2E}\hat{c}_2[E_k,s+i(\Delta_E-\Delta)]\} , \\
(is-\Delta_{ba})\hat{c}_b(s+i\Delta_{ba}) &= i+V_{bg}\hat{c}_g(s+i\Delta_{ga})+V_{ba}\hat{c}_a(s) \\
&\quad + \int_0^\infty dE_k\{V_{b,1E}\hat{c}_1(E_k,s+i\Delta_E)\} , \\
(is-\Delta_{ga})\hat{c}_g(s+i\Delta_{ga}) &= V_{gb}\hat{c}_b(s+i\Delta_{ba}) ,
\end{aligned}
\tag{7}
$$

where the circumflex symbol indicates the Laplace transform.

In solving these coupled equations we encounter numerous "self-energy" integrals of the form

$$
\Sigma^{ij}_{\alpha\beta}(is) = \int_0^\infty \frac{V_{\alpha,jE}V_{jE,\beta}}{is-\Delta E}dE_k , \quad \alpha,\beta=a,b , \quad j=1,2 \tag{8}
$$

which represent an effective coupling between discrete states $|\alpha\rangle$ and $|\beta\rangle$ (which may be the same state) through the continuum $\{|j,E_k\rangle\}$. Considerable simplification occurs if we assume Σ to be slowly varying enough that we can ignore small changes in the real part of their arguments and approximate, for example, $\Sigma^2_{aa}(is-\Delta) \approx \Sigma^2_{aa}(is)$. After algebraic manipulation we find, defining $z=is+E_a$,

$$
\begin{aligned}
&\hat{c}_a(s) = i\frac{(z-E_g-2\omega)\Lambda_{ab}}{P(z)} , \quad \hat{c}_g(s+i\Delta_{ga}) = i\frac{(z-E_a-\Lambda_{aa})V_{gb}}{P(z)} , \\
&\hat{c}_b(s+i\Delta_{ba}) = i\frac{(z-E_g-2\omega)(z-E_a-\Lambda_{aa})}{P(z)} , \quad \hat{c}_1(E_k,s+i\Delta_E) = \frac{iR(z)}{P(z)[(z-E_k-E_1)(z-E_k-E_1+\Delta)-V_{12}V_{21}]} , \\
&\hat{c}_2(E_k,s+i(\Delta_E-\Delta)) = \frac{1}{z-E_k-E_1+\Delta}[V_{21}\hat{c}_1(E,s+i\Delta_E)+V_{2E,a}\hat{c}_a(s)] ,
\end{aligned}
\tag{9}
$$

where

$$
\begin{aligned}
R(z) &= (z-E_g-2\omega)\{[(z-E_k-E_1+\Delta)V_{1E,a}+V_{12}V_{2E,a}]\Lambda_{ab}+(z-E_k-E_1+\Delta)V_{1E,b}(z-E_a-\Lambda_{aa})\} , \\
P(z) &= (z-E_b-\omega-\Lambda_{bb})(z-E_g-2\omega)(z-E_a-\Lambda_{aa})-|V_{bg}|^2(z-E_a-\Lambda_{aa})-(z-E_g-2\omega)\Lambda_{ba}\Lambda_{ab} ,
\end{aligned}
\tag{10}
$$

and where

$$
\Lambda_{aa} = \Sigma^{22}_{aa}(z)+\Sigma^{11}_{aa}(z) , \quad \Lambda_{ab} = V_{ab}+\Sigma^{11}_{ab}(z) , \quad \Lambda_{bb} = \Sigma^{11}_{bb}(z) . \tag{11}
$$

In these expressions Λ can be recognized as the level-shift operator in the space of discrete states in the absence of any continuum-continuum coupling. We note that the expressions for the discrete-state coefficients are independent of V_{12}, as a consequence of our approximations, so that the discrete-state populations are unaffected by the continuum-continuum δ-function coupling.

The inverse Laplace transforms can now be considered. We make the pole approximation $\Sigma^{ij}_{\alpha\beta}(E+i0) = -i\pi V_{\alpha,jE}V_{jE,\beta}$, and we ignore the energy dependence of the discrete-state–continuum matrix elements. The integrands for the discrete-state amplitudes then feature only simple poles, which lie at the three zeros z_n of $P(z)$ in the fourth quadrant of the complex z plane. The

discrete-state population amplitudes are

$$\langle a|\psi(t)\rangle=\sum_{n=1}^{3} e^{-iz_n t}\frac{(z_n-E_g-2\omega)\Lambda_{ab}}{P'(z_n)} ,$$
$$\langle g|\psi(t)\rangle=\sum_{n=1}^{3} e^{-iz_n t}\frac{(z_n-E_a-\Lambda_{aa})V_{gb}}{P'(z_n)} , \quad (12)$$
$$\langle b|\psi(t)\rangle=\sum_{n=1}^{3} e^{-iz_n t}\frac{(z_n-E_g-2\omega)(z_n-E_a-\Lambda_{aa})}{P'(z_n)} .$$

The integrand for the continuum population amplitude c_1 has poles at the z_n and also has real-axis poles at the two energies $E_\pm$ which satisfy

$$(z-E_k-E_1)(z-E_k-E_1+\Delta)-V_{12}V_{21}=0 . \quad (13)$$

The population amplitude for the first continuum is thus

$$c_1(E_k,t)=e^{i(E_k+E_1)t}\left\{\sum_{n=1}^{3} e^{-iz_n t}\frac{R(z_n)}{P'(z_n)(z_n-E_+)(z_n-E_-)}+e^{-iE_+ t}\frac{R(E_+)}{P(E_+)(E_+-E_-)}\right.$$
$$\left.+e^{-iE_- t}\frac{R(E_-)}{P(E_-)(E_--E_+)}\right\} . \quad (14)$$

Finally, the population amplitude in the second continuum can be obtained taking the inverse Laplace transform of Eq. (9) for $\hat{c}_2$. After minor simplification we obtain

$$c_2(E_k,t)=e^{i(E_k+E_1-\Delta)t}\left\{\frac{2V_{12}}{\Omega}\left[e^{-iE_+ t}\frac{R(E_+)}{(\Omega+\Delta)P(E_+)}+e^{-iE_- t}\frac{R(E_-)}{(\Omega-\Delta)P(E_-)}\right]\right.$$
$$+V_{12}\sum_{n=1}^{3} e^{-iz_n t}\frac{R(z_n)}{(z_n-E_1-E_k+\Delta)P'(z_n)(z_n-E_+)(z_n-E_-)}$$
$$\left.+V_{2E,a}\Lambda_{ab}\sum_{n=1}^{3} e^{-iz_n t}\frac{z_n-E_g-2\omega}{(z_n-E_1-E_k+\Delta)P'(z_n)}\right\} , \quad (15)$$

where

$$\Omega=\sqrt{\Delta^2+4V_{12}^2} \quad (16)$$

denotes an effective Rabi frequency for the $|1\rangle\leftrightarrow|2\rangle$ coupling.

The total population density at kinetic energy E_k is $S(E_k)=|c_1(E_k,t)|^2+|c_2(E_k,t)|^2$ and can easily be calculated if particular numerical values are chosen for the various atomic and laser parameters. We do not write out the expression because of its length.

These equations complete the formal solution for our essential-states model. We defer most discussion of the general results of the solution until we have considered several simplified cases in which particular couplings have been set to zero and which illustrate the importance of V_{12} most clearly.

Because the z_n are complex with $\mathrm{Im}[z_n]<0$, all exponentials $\exp(-iz_n t)$ go asymptotically to zero at long times. In examining the simplified cases we shall focus our attention on the kinetic-energy spectra at these long times at which no population remains in the discrete states.

Before proceeding to special cases, we introduce notation similar to that used in some studies [9] of laser-induced autoionization in which Γ, the rate of autoionization of state $|a\rangle$, is used as a normalizing standard for the various key rates,

$$\Gamma=2\pi|V_{a,1E}|^2 , \quad \gamma=\frac{|V_{a,2E}|^2}{|V_{a,1E}|^2} ,$$
$$\alpha=\frac{E_b+\omega-E_a}{(\Gamma/2)} , \quad \xi=\frac{|V_{b,1E}|^2}{|V_{a,1E}|^2} ,$$
$$q=\frac{V_{ab}}{\pi V_{a,1E}V_{b,1E}} , \quad \varepsilon=\frac{E_1+E_k-E_a}{(\Gamma/2)} , \quad (17)$$
$$\Delta'=\frac{\Delta}{(\Gamma/2)} , \quad \Omega'=\frac{\Omega}{(\Gamma/2)} .$$

Here γ represents the relative decay rate of $|a\rangle$ by photoabsorption, α is the detuning of the laser from the $|b\rangle\leftrightarrow|a\rangle$ resonance, and ξ is the relative rate for $|b\rangle\rightarrow\{|1,E_k\rangle\}$ transitions. ε and q are as defined by Fano [7].

III. LONG-TIME KINETIC-ENERGY SPECTRA FOR SIMPLIFIED SYSTEMS

The ground state $|g\rangle$ was included above for completeness and because it can be important in modeling particular systems. However, its inclusion does complicate the formalism and it is not necessary for describing the primary effects of interest in this paper. Consequently, in the following analysis we shall set $V_{bg}=0$. This has the effect of removing the ground state from the essential-

state model. There are several interesting subcases, as follows:

A. $V_{a,2E}=0$

We consider first a situation in which $V_{a,2E}=0$. There is then no photoabsorption from $|a\rangle$, and the continuum $\{|2,E_k\rangle\}$ is only accessible from the δ-function coupling with the $\{|1,E_k\rangle\}$ continuum. In the limit $V_{12}\rightarrow 0$ no population can reach the second continuum, and the photoelectron spectrum can be written rather simply as

$$\tilde{S}^0(E_k)=\lim_{t\rightarrow\infty}|c_1(E_k t)|^2=|\phi(\varepsilon)|^2 ,$$

where

$$\phi(\varepsilon)=\left[\frac{2\xi}{\pi\Gamma}\right]^{1/2}\frac{(\varepsilon+q)}{\tilde{P}(\varepsilon)} \tag{18}$$

with

$$\begin{aligned}\tilde{P}(\varepsilon)&=P(\varepsilon)|_{V_{a,2E}=0}=[(\varepsilon-\alpha)\varepsilon-\xi q^2)]\\&\quad+i[\xi\varepsilon+(\varepsilon-\alpha)+2q\xi]\\&=\varepsilon^2+[-\alpha+i(\xi+1)]\varepsilon-q^2\xi+i(2q\xi-\alpha)\\&\equiv(\varepsilon-\tilde{z}_1)(\varepsilon-\tilde{z}_2) .\end{aligned} \tag{19}$$

[We use a superscript 0 to indicate that $V_{12}=0$ and a tilde ($\sim$) to indicate $V_{a,2E}=0$ in writing quantities that have different forms when these respective matrix elements are nonzero.] Equations (18) and (19) reproduce the standard result for laser-induced autoionization in the absence of coherence-destroying effects. The spectrum exhibits peaks at the real parts of each of the two roots $\tilde{z}_n$ and peak widths $2|\mathrm{Im}(\tilde{z}_n)|$. As has been extensively discussed in the literature [8], these peaks can have very different widths and heights. More specifically, one peak grows progressively narrower and taller as its center approaches the Fano minimum at $\varepsilon=-q$. The two complex energies $\tilde{z}_n$ can be interpreted as representing "decaying dressed states" of energies $\mathrm{Re}(\tilde{z}_n)$ and decay rates $2|\mathrm{Im}(\tilde{z}_n)|$. The area under the curve for a given peak can be associated with the initial population of the relevant dressed state and depends on the extent to which the initial state of the system $|b\rangle$ is represented in the dressed state. A sample spectrum is shown as the solid curve of Fig. 2, and reproduces part of Fig. 3 of Ref. [9a]. Because there is no coupling to the $\{|2,E_k\rangle\}$ continuum, all the population resides in the $\{|1,E_k\rangle\}$ continuum.

If we now allow V_{12} to be nonzero, $|c_1(E_k,t)|^2$ gives the long-time limit kinetic-energy spectrum in the $\{|1,E_k\rangle\}$ continuum as

$$\tilde{S}_1(E_k)=\left|\frac{\Omega+\Delta}{2\Omega}\phi(\varepsilon-\Delta'/2+\Omega'/2)+\frac{\Omega-\Delta}{2\Omega}\phi(\varepsilon-\Delta'/2-\Omega'/2)e^{i\Omega t}\right|^2 . \tag{20}$$

This result corresponds to that presented in Refs. [10] and [11], except that in the present work we have introduced dimensionless arguments for ϕ. Each peak at $\mathrm{Re}(\tilde{z}_n)$ is replaced by a doublet at $\mathrm{Re}(\tilde{z}_n)-\Delta'/2\pm\Omega'/2$, with relative heights determined by the multiplicative factors $(\Omega\pm\Delta)/(2\Omega)$. There is also a time-dependent cross term which persists for all time.

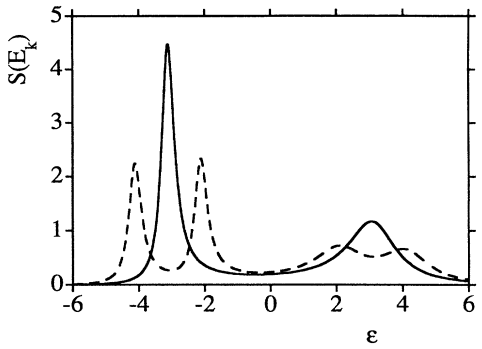

FIG. 2. Photoelectron energy spectrum $S(E_k)$ vs ε for $V_{12}=0$ (solid curve) and $V_{12}=\Gamma/2$ (dashed curve), in units of $1/(\pi\Gamma)$. The zero of ε corresponds to the energy of the autoionizing state. Parameters are $q=10$, $\xi=0.10$, $\Delta=0$, and $\alpha=0$.

The V_{12} coupling allows population to reach the second continuum, with $|c_2(E_k,t)|^2$ giving the long-time kinetic-energy spectrum

$$\tilde{S}_2(E_k)=\left|\frac{V_{12}}{\Omega}\phi(\varepsilon-\Delta'/2+\Omega'/2)-\frac{V_{12}}{\Omega}\phi(\varepsilon-\Delta'/2-\Omega'/2)e^{i\Omega t}\right|^2 . \tag{21}$$

Thus the population in the second continuum is peaked about the same kinetic energies as in the first continuum. The sum of the two population densities at long times can be shown to simplify to the time-independent result

$$\begin{aligned}\tilde{S}(E_k)&=\tilde{S}_1(E_k)+\tilde{S}_2(E_k)\\&=\frac{\Omega+\Delta}{2\Omega}|\phi(\varepsilon-\Delta'/2+\Omega'/2)|^2\\&\quad+\frac{\Omega-\Delta}{2\Omega}|\phi(\varepsilon-\Delta'/2-\Omega'/2)|^2 .\end{aligned} \tag{22}$$

Recalling that the long-time kinetic-energy spectrum for $V_{12}=0$ is simply $|\phi(\varepsilon)|^2$, we conclude that the net effect of the V_{12} coupling on the long-time kinetic-energy spectrum is simply a splitting and shifting of the $V_{12}=0$ spectra. The two new peaks are separated in energy by Ω and their relative heights are given by the multiplicative factors $(\Omega\pm\Delta)/(2\Omega)$. This result is illustrated in Fig. 2. Because Δ is chosen to equal zero for this plot, the two new peaks have equal height.

In general, the splitting of a spectral peak is evident whenever Ω becomes greater than the $V_{12}=0$ linewidth of the peak. In Fig. 2, Ω is large ($=\Gamma$, so $\Omega'=2$) and the splitting is evident for both peaks. If one of the $V_{12}=0$ peaks were every narrow, as can happen if it lies close to the Fano minimum, then the splitting predicted by Eq. (22) would become noticeable for much smaller values of Ω.

The time dependences of $\tilde{S}_1$ and $\tilde{S}_2$ in Eqs. (20) and (21) indicate that there are Rabi oscillations between the two continua which persist for all time. The manifestation of these oscillations in the spectra is shown in Fig. 3 for a sequence of times over one laser cycle for the parameters of Fig. 2. Because population enters the first continuum over an extended time interval, the oscillations are not in phase and populations of the individual continua never go all the way to zero or to one.

As suggested by Refs. [10] and [11], our results are easily explained by dressing the final states of the system. The positive-ion states $|1\rangle$ and $|2\rangle$ combine to form dressed states $|+\rangle$ and $|-\rangle$ of energy $E_{D\pm}=[E_1+(E_2-\omega)]/2\pm\Omega/2=E_1-\Delta/2\pm\Omega/2$ (and $E_{D\pm}+\omega$). These energies are related to the total energies $E_\pm$ which solve Eq. (13) by $E_\pm=E_{D\pm}+E_k$. One can describe the final states of the ionized system using either the undressed continua $\{|1,E_k\rangle\}$ and $\{|2,E_k\rangle\}$ or the dressed continua $\{|+,E_k\rangle\}$ and $\{|-,E_k\rangle\}$. In the former case there are Rabi oscillations between the continua which continue indefinitely [thereby giving rise to the time dependence of Eqs. (20) and (21) and shown in Fig. 3]. If one describes the final states using the dressed continua no such oscillations occur, but the thresholds of the two continua are slightly shifted from the undressed case. Of course, both descriptions lead to the same overall kinetic-energy spectrum (22). The shifts in Eq. (22) as well as the relative peak heights are precisely what one would expect from an Autler-Townes dressing of the final states. We shall develop the dressed-state interpretation of (22) more fully after presentation of the spectrum for the more complicated case of $V_{a,2E}\neq 0$.

B. $V_{a,2E}\neq 0$

The effect of photoabsorption from $|a\rangle$ for $V_{12}=0$ has been extensively discussed in the literature. The new decay channel can shift the spectral peaks in the $\{|1,E_k\rangle\}$ continuum as well as alter their widths, generally broadening any narrow features. In addition, the spectrum within the new decay channel can now be considered, and the overall kinetic-energy spectrum is the sum of the two individual spectra. Mathematical expressions for the individual kinetic-energy spectra when $V_{12}=0$ are

$$S_1^0(E_k)=\lim_{t\to\infty}|c_1(E_k,t)|^2=|\phi_1(\varepsilon)|^2 ,$$

$$S_2^0(E_k)=\lim_{t\to\infty}|c_2(E_k t)|^2=|\phi_2(\varepsilon-\Delta')|^2 ,$$

where

$$\phi_1(\varepsilon)=\left[\frac{2\xi}{\pi\Gamma}\right]^{1/2}\frac{(\varepsilon+q)+i\gamma}{P(\varepsilon)} , \tag{23}$$

$$\phi_2(\varepsilon)=\left[\frac{2\xi}{\pi\Gamma}\right]^{1/2}\frac{\sqrt{\gamma}(q-i)}{P(\varepsilon)} , \tag{24}$$

$$P(\varepsilon)=[(\varepsilon-\alpha)\varepsilon-\xi(\gamma+q^2)] +i[\xi\varepsilon+(1+\gamma)(\varepsilon-\alpha)+2q\xi] ,$$

The total kinetic-energy spectrum is then

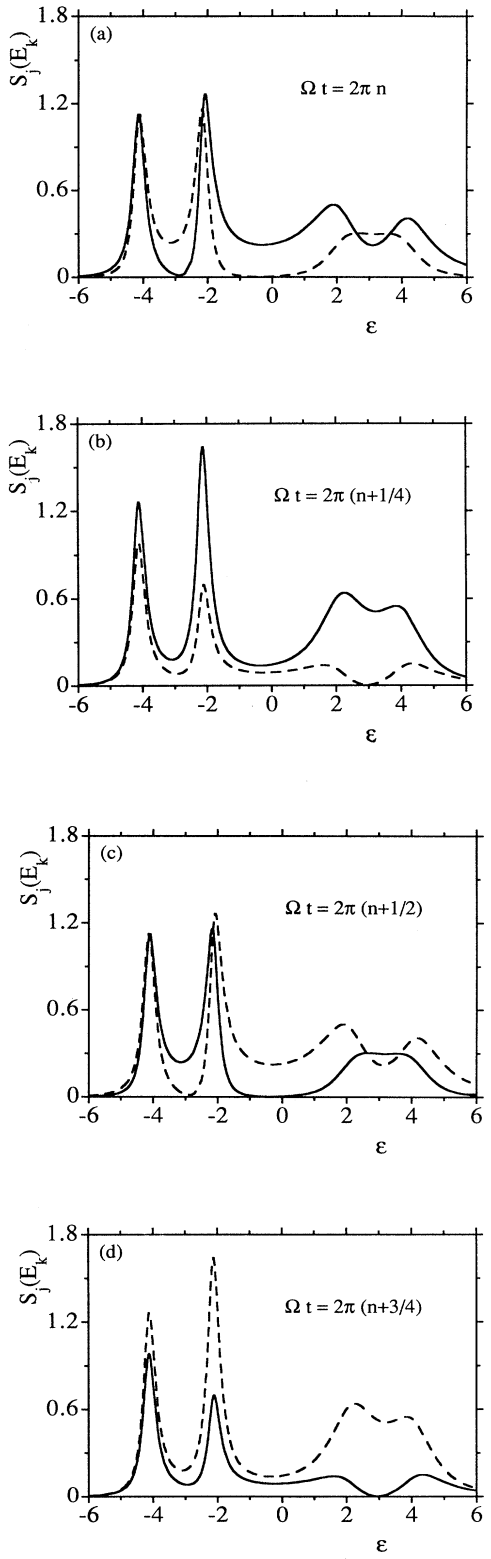

FIG. 3. Long-time photoelectron energy spectra $S_1(E_k)$ (solid curve) and $S_2(E_k)$ (dashed curve) in units of $1/(\pi\Gamma)$ at a sequence of times separated by one-quarter Rabi cycle for the conditions of Fig. 2 with $V_{12}=\Gamma/2$. The sum of the two curves is constant and corresponds to the dashed curve of Fig. 2. Here n represents any large positive integer.

$$S(E_k)=S_1^0(E_k)+S_2^0(E_k)$$
$$=|\phi_1(\varepsilon)|^2+|\phi_2(\varepsilon-\Delta')|^2 . \quad (25)$$

These results are the same as those for laser-induced autoionization systems, with $S_1^0(E_k)$ representing the modified decay spectrum in the original channel, and $S_2^0(E_k)$ the spectrum in the new channel, regardless of whether the new channel is opened by photoabsorption into a different electron continuum [15], as in the present study, or spontaneous radiative decay [9], or even autoionization into a second electron continuum [16].

When V_{12} is nonzero, the long-time limit kinetic-energy spectrum $S(E_k)=S_1(E_k)+S_2(E_k)$ can be written, after some algebraic manipulation,

$$S(E_k)=\left|\left[\frac{\Omega+\Delta}{2\Omega}\right]^{1/2}\phi_1\left[\varepsilon-\frac{\Delta'}{2}+\frac{\Omega'}{2}\right]+\mathrm{sgn}[V_{12}]\left[\frac{\Omega-\Delta}{2\Omega}\right]^{1/2}\phi_2\left[\varepsilon-\frac{\Delta'}{2}+\frac{\Omega'}{2}\right]\right|^2$$
$$+\left|\left[\frac{\Omega-\Delta}{2\Omega}\right]^{1/2}\phi_1\left[\varepsilon-\frac{\Delta'}{2}-\frac{\Omega'}{2}\right]-\mathrm{sgn}[V_{12}]\left[\frac{\Omega+\Delta}{2\Omega}\right]^{1/2}\phi_2\left[\varepsilon-\frac{\Delta'}{2}-\frac{\Omega'}{2}\right]\right|^2 . \quad (26)$$

The mixing of the two atomic decay channels is clearly apparent since ϕ_1 and ϕ_2 do not appear in separate modulus squared terms as in (25). We will show in Sec. III C below that each modulus squared term represents the population density in one of the dressed continua. First, though, we compare the result (26) with our earlier result (22) to which it collapses as $\gamma\to 0$ (so that $\phi_2\to 0$ and $\phi_1\to\phi$). The most significant difference is the superposing of ϕ_1 and ϕ_2 within each modulus squared. We note that because ϕ_1 and ϕ_2 have the same arguments and because peak structures for both $|\phi_1(\varepsilon)|^2$ and $|\phi_2(\varepsilon)|^2$ are determined by the denominator $P(\varepsilon)$ [Eqs. (23) and (24)], the superposing of ϕ_1 and ϕ_2 does not lead to any new peaks in $S(E_k)$. As before, V_{12} splits each peak into a doublet, with separation Ω'. However, the superposing of ϕ_1 and ϕ_2 is different in each modulus squared, and consequently the relative heights of the doublet peaks can be very different. For example, for $\Delta=0$, the two superpositions are proportional to

$$\phi_1(\varepsilon)\pm\phi_2(\varepsilon)=\left[\frac{2\xi}{\pi\Gamma}\right]^{1/2}\times\left[\frac{(\varepsilon+q\pm\mathrm{sgn}[V_{12}]\sqrt{\gamma}q)+i(\gamma\mp\sqrt{\gamma})}{P(\varepsilon)}\right] . \quad (27)$$

The zero of the real part of the numerator does not occur at $\varepsilon=-q$ but at $\varepsilon=-(q\pm\mathrm{sgn}[V_{12}]\sqrt{\gamma}q)$.

These results are illustrated in Fig. 4, where we have the same parameters as in Figs. 2 and 3 ($q=10$), but allow for nonzero γ. The right-hand peak of the doublet is nearly destroyed for $\gamma=0.1$ ($\sqrt{\gamma}q\simeq 3$). If V_{12} had the opposite sign, then the left-hand peak would be destroyed instead. We conclude that photoionization from the autoionizing state can destroy the core-coherence doublets if the field is too strong.

C. Dressed-state analysis

The above results for the spectra are consistent with what one would obtain by dressing the final states of the positive ion. The connection is perhaps most apparent if one works with a quantized radiation field rather than a time-dependent, classical radiation field. In particular the states $|1,N\omega\rangle$ and $|2,(N-1)\omega\rangle$ are coupled by a laser of detuning Δ, and form dressed states

$$|+\rangle=\left[\frac{\Omega+\Delta}{2\Omega}\right]^{1/2}|1,N\omega\rangle+\mathrm{sgn}[V_{12}]\left[\frac{\Omega-\Delta}{2\Omega}\right]^{1/2}|2,(N-1)\omega\rangle ,$$
$$|-\rangle=\left[\frac{\Omega-\Delta}{2\Omega}\right]^{1/2}|1,N\omega\rangle-\mathrm{sgn}[V_{12}]\left[\frac{\Omega+\Delta}{2\Omega}\right]^{1/2}|2,(N-1)\omega\rangle . \quad (28)$$

The dressed continua then have the form $\{|+,E_k\rangle\}$ and $\{|-,E_k\rangle\}$. These continua are orthonormal and are not coupled.

In general, the energy spectrum of a system initially in state some state $|i\rangle$ decaying into an isolated continuum $|E\rangle$ (where E denotes the *total* energy of the continuum state) can be written [17] in the form

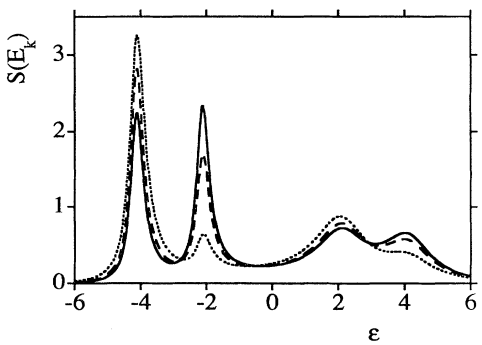

FIG. 4. Long-time photoelectron energy spectrum S in units of $1/(\pi\Gamma)$ vs ε for conditions of Fig. 2 with $V_{12}=\Gamma/2$, but with $\gamma=0$ (solid curve), 0.01 (dashed curve), and 0.1 (dotted curve).

$$K(E)=\left|\sum_n \langle E|V|n\rangle\langle n|G(E+i0)|i\rangle\right|^2, \tag{29}$$

where $G(z)$ denotes the resolvent or Green's operator, $G(z)=(z-H)^{-1}$, and where the sum is over all the discrete states of the system. (By an "isolated" continuum, we mean a continuum that is not coupled to any other continua.) For our dressed continua,

$$\langle \pm,E_k|V|n\rangle=\left[\frac{\Omega\pm\Delta}{2\Omega}\right]^{1/2}\langle 1,N\omega;E|V|n\rangle \pm\mathrm{sgn}[V_{12}]\left[\frac{\Omega\mp\Delta}{2\Omega}\right]^{1/2}\times\langle 2,(N-1)\omega;E|V|n\rangle , \tag{30}$$

so for each individual dressed continuum (29) gives

$$K_{\pm}(E)=\left|\sum_n\left[\left[\frac{\Omega\pm\Delta}{2\Omega}\right]^{1/2}\langle 1,N\omega;E|V|n\rangle\langle n|G(E+i0)|i\rangle \pm\mathrm{sgn}[V_{12}]\left[\frac{\Omega\mp\Delta}{2\Omega}\right]^{1/2}\langle 2,(N-1)\omega;E|V|n\rangle\langle n|G(E+i0)|i\rangle\right]\right|^2 . \tag{31}$$

One can show that in the pole approximation discrete state–discrete state matrix elements $\langle n|G(E+i0)|i\rangle$ are the same regardless of whether the continuum-continuum δ-function coupling is included, in accord with our earlier conclusion that the δ-function coupling does not affect the time development of the discrete-state populations. We thus recognize $\sum_n\langle 1,N\omega;E|V|n\rangle\langle n|G(E+i0)|i\rangle$ as the spectral amplitude for decay of $|i\rangle$ into the $|1,N\omega;E\rangle$ continuum for the case of zero continuum-continuum coupling. This spectral amplitude corresponds to what we have denoted by ϕ_1 above. When the distinction between total energy of the continuum state and the kinetic energy of the outgoing electron is taken into account, Eq. (31) gives

$$K_{\pm}(E)=\left|\left[\frac{\Omega\pm\Delta}{2\Omega}\right]^{1/2}\phi_1(\varepsilon-\Delta'/2\pm\Omega'/2) \pm\mathrm{sgn}[V_{12}]\left[\frac{\Omega\mp\Delta}{2\Omega}\right]^{1/2}\times\phi_2(\varepsilon-\Delta'/2\pm\Omega'/2)\right|^2 . \tag{32}$$

The sum $K_+(E)$ and $K_-(E)$ reproduces Eqs. (26) for the full kinetic-energy spectrum, and allows us to identify the respective mod squared terms in (26) with the spectra in

IV. ESSENTIAL-STATES SOLUTION AT FINITE TIMES: APPLICATION TO ONE-DIMENSIONAL HELIUM

Thus far our analysis has concentrated on the kinetic-energy spectra at long times. In this section, we use the full essential-states solution [Eqs. (14) and (15)] to study the spectra at shorter times. For definiteness, we choose parameters that are appropriate for one-dimensional helium, as was done in Ref. [11]. This choice allows us to compare the predictions of the essential-states model with the exact numerical solution [18] of the time-dependent Schrödinger equation for the model atom. The initial state $|b\rangle$ corresponds to the first-excited state of the atom, which can be denoted by $|1,2\rangle$ even though the electron-electron interaction prevents the state from being a product state. Similarly, the ground state $|g\rangle$ can be denoted $|1,1\rangle$. For the autoionizing state $|a\rangle$ we choose the lowest-energy autoionizing state $|2,2\rangle$. We use specifically the state denoted by $|+a\rangle$ in Ref. [14]. This state is obtained by diagonalizing the Hamiltonian matrix within a limited Hilbert-space spanned by $He^+\otimes He^+$ product states, but with the final-state continuum $|1\rangle\otimes|E\rangle$ excluded. The decay continuum $|1,E_k\rangle$ is obtained by diagonalizing the Hamiltonian in the complementary, $|1\rangle\otimes|E\rangle$ subspace.

Having defined our states, appropriate dipole and autoionizing matrix elements can be calculated. We treat $V_{b,1E}$ and $V_{a,1E}$ as independent of energy, and we use their values at the energy of the autoionizing state, but we treat $V_{a,2E}$ (which varies more rapidly with continuum energy) as an adjustable, ω-dependent parameter. The Fano q parameter for the resonance is approximately -20 [19].

In the present work, we are interested in examining the core-coherence effect without superposing extraneous effects such as can arise from laser turn on and turn off. Consequently, in our numerical study we use a rapid turn on and laser pulses that are long enough that laser turn-on and turn-off effects are unimportant. In particular, we linearly ramp the turn on and turn off over 2 laser cycles and typically consider 40-cycle pulses. This turn on improves on the assumption of instantaneous turn on of the essential states analysis, while still being short enough not to mask the central focus of this work. We comment that Ref. [10] uses a $\sin^2$ pulse in its numerical study of the core-coherence effect.

We consider specifically a laser field of amplitude 0.075 a.u. Photoelectron kinetic-energy spectra are shown in Figs. 5–7 for three different laser frequencies. Part (a) of each figure shows the predictions of our essential-states model both neglecting (dashed curves) and including (solid curves) the V_{12} core coupling, while part (b) of each figure shows the full numerical solution for the same laser parameters. In Fig. 5, the laser is resonant with the neutral atom $|b\rangle-|a\rangle$ ($|1,2\rangle-|2,2\rangle$) transition frequency, so that the dashed curve of Fig. 5(a) exhibits the familiar

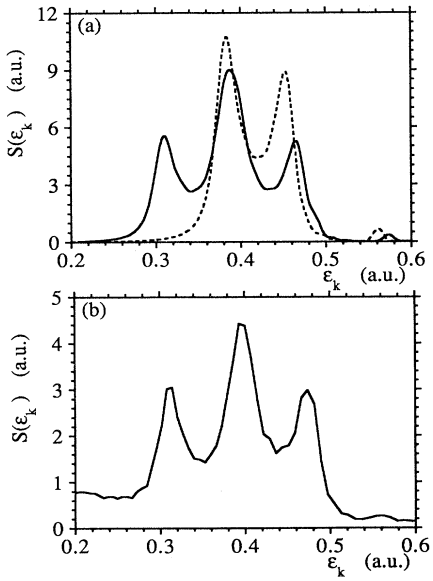

FIG. 5. (a) Kinetic-energy spectra of essential-states model for laser field strong $F=0.075$ and frequency $\omega=0.65$ with (solid curve) and without (dashed curve) the V_{12} coupling. (b) Kinetic-energy analysis of exact numerical solution. Laser pulse duration is 40 cycles. Atomic matrix elements to two significant figures are (in a.u.) $V_{12}=0.40F$, $V_{b,1E}=01.0F$, $V_{a,1E}=-0.089$, $V_{a,2E}=-0.46F$, $V_{ba}=0.57F$, and $V_{gb}=0.55F$. In terms of parameters of Sec. III, $\Gamma=0.050$, $\gamma=0.15$, $\xi=0.0072$, $\Delta'=2.5$, $V_{12}(\Gamma/2)=1.2$, and $q=-20$.

asymmetric doublet of laser-induced autoionization. When the V_{12} core coupling is included each of these peaks is split into a doublet, but because of overlap the combined spectrum takes on a triplet form. The laser frequency used in Fig. 6 corresponds to the $|1\rangle-|2\rangle$ core resonance frequency (Fig. 6 reproduces Fig. 2 of Ref. [11]), and the figure clearly shows the coherence-transfer

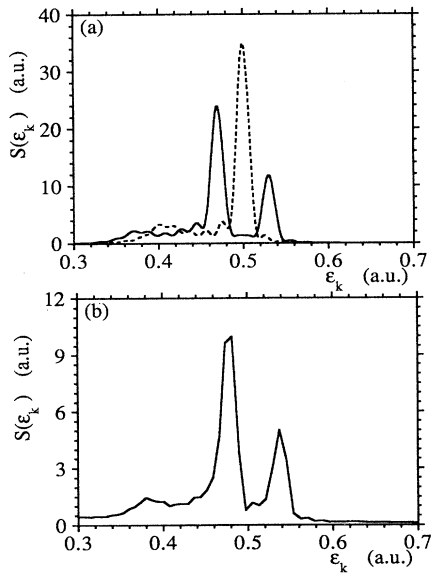

FIG. 6. Similar to Fig. 5, except $\omega=0.71$, the core resonance frequency, and $V_{a,2E}=-0.17F(\Delta'=0,\alpha=2.5,\gamma=0.021)$.

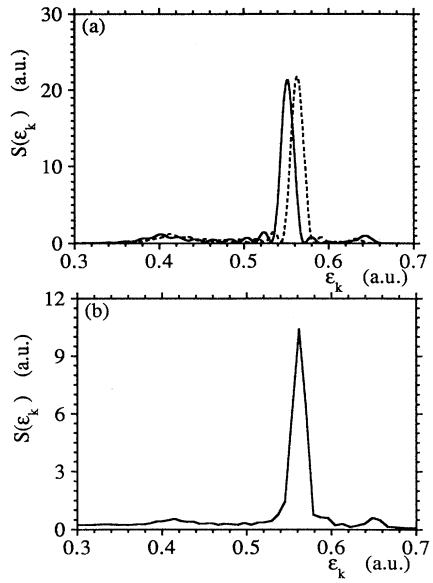

FIG. 7. Similar to Fig. 5, except $\omega=0.78$, and $V_{a,2E}=-0.13F(\Delta'=2.8,\alpha=5.3,\gamma=0.012)$.

effect. The frequency chosen for Fig. 7 is not resonant with any atomic transitions, and the spectrum is characterized by a single dominant peak regardless of whether V_{12} is included.

As predicted above, each spectral peak in our essential-states model is split into a doublet when the core coupling is included. In addition, the relative peak heights in each case are consistent with the exact numerical solution. These observations provide substantial justification for the use of the δ coupling in our model. As mentioned in [11], the difference in scale between the essential states predictions and the full numerical solution can be explained by noting that the graph of the numerical solution shows only one component of a sequence of above-threshold ionization peaks, while the essential-states model neglects couplings needed to obtain a sequence of peaks.

In Figs. 8–10, we present the time development of various quantities. In all cases, we follow the convention of Figs. 5–7 of plotting essential-states results in parts (a) and exact numerical solutions in parts (b). In these figures, the laser frequency is fixed at the core-resonance frequency $\omega=0.71$ a.u. used in Fig. 6.

Figure 8(a) shows our essential-states prediction for the time development of the population in the initial state. Because of the fairly large laser strength of $F=0.075$ a.u. and our tuning to the core resonance rather than the autoionizing resonance, Rabi oscillations involving the initial state are very limited. As mentioned above, all discrete-state populations are independent of V_{12}. The ground sate has between excluded ($V_{bg}=0$) in the dashed curve but included ($V_{bg}\neq 0$) in the solid curve. In the latter case we observe that some population oscillates between the initial and ground states. Figure 8(b) shows the full numerical solution for the development of the population in the initial state. The slight horizontal shift between Figs. 8(a) and 8(b) results from ramping the turn on

in the numerical solution.

In analyzing the populations in the first and second continua, we anticipate Rabi oscillations between the continua as the core electron oscillates between the states $|1\rangle$ and $|2\rangle$. Figure 9(b) shows the output of the exact numerical solution for the total probability P_1 to have at least one electron in the ground state of He^+, i.e., the component of the population that can be projected onto (properly symmetrized) $He^+ \otimes He^+$ *product* states $|1\rangle \otimes |j\rangle$, where j is arbitrary. Since the energy of the initial state $|b\rangle$ is well below the energy of states $|2\rangle \otimes |2\rangle$ and higher, the initial state is composed almost entirely of states $|1\rangle \otimes |j\rangle$ so that at $t=0$, Fig. 9(b) shows the total population nearly one. At longer times, the states $|1\rangle \otimes |1\rangle$ and $|1\rangle \otimes |2\rangle$ become less populated so that the population depicted in Fig. 9(b) corresponds more closely with the population of what we have called the first continuum.

For comparison we include, as Fig. 9(a), the time development of the sum of the populations of $|b\rangle$, $|g\rangle$, and $|1,E_k\rangle$ in our essential-states model. The extent to which Fig. 9(a) replicates Fig. 9(b) particularly in showing the Rabi oscillations provides additional justification for the essential-states model. The slight shift between Figs. 9(a) and 9(b) again results from ramping the turn on.

Figure 10(b) shows the population P_2 that can be projected onto product states $|2\rangle \otimes |j\rangle$, where j is arbitrary, for the numerical solution. Because the initial state $|b\rangle$ is not identically a product $|1\rangle \otimes |2\rangle$ but includes projections onto states $|1\rangle \otimes |j\rangle$, $j \neq 2$, and P_2 does not equal one at $t=0$. As time elapses the Rabi oscillations characteristic of the second continuum become evident.

For comparison we include as Fig. 10(a) the development of the total population in $|a\rangle$ and $|2,E_k\rangle$ as predicted by our essential-states model. We exclude the initial state $|b\rangle$ because, as mentioned, not all of $|b\rangle$ can be projected onto states $|2\rangle \times |j\rangle$ [about 70% as suggested by Fig. 10(b)]. Therefore, we expect Fig. 10(a) to correspond to Fig. 10(b) only for long times when the discrete states are unpopulated. Indeed, our model accurately predicts the Rabi oscillations which occur at longer times.

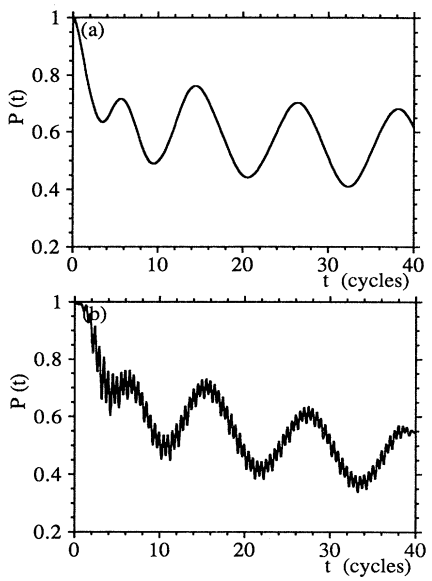

FIG. 9. (a) Predictions of essential-states model for the combined populations of the ground state $|g\rangle$, the first-excited state $|b\rangle$, and the $|1,E_k\rangle$ continuum. (b) Numerical calculation of the probability $P_1(t)$ that at least one electron lies in the ground state of He^+. Parameters are as in Fig. 6.

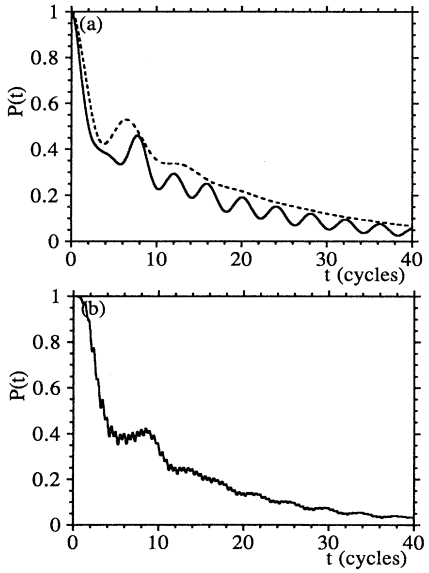

FIG. 8. (a) Essential-states population $|\langle b|\psi(t)\rangle|^2$ vs time when the ground state is excluded ($V_{bg}=0$, dashed curve) and included ($V_{bg}\neq 0$). (b) Population in the initial state for full numerical solution. All parameters are as in Fig. 6.

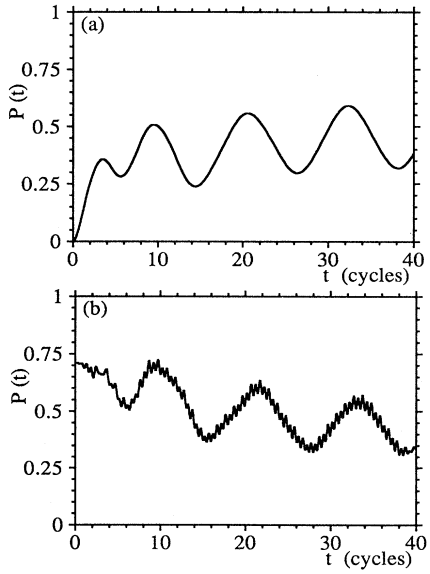

FIG. 10. (a) Population of the $|2,E_k\rangle$ continuum versus time in the essential-states calculation. (b) Numerical calculation of the population P_2 of the first-excited state of He^+. Parameters are as in Fig. 6.

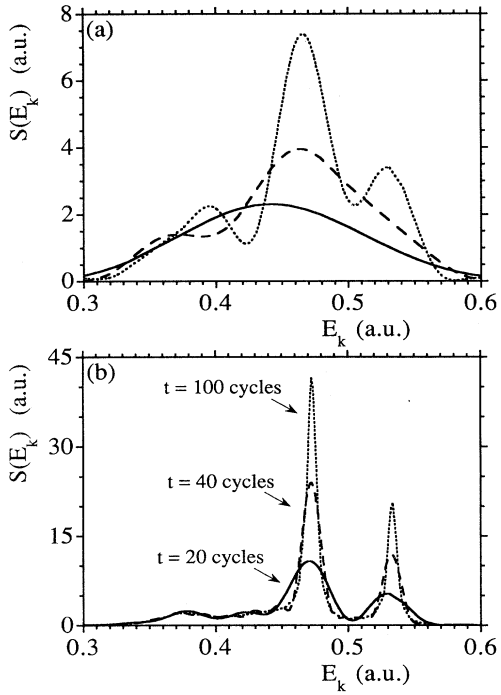

FIG. 11. Time development of the photoelectron spectrum $S(E_k)$ in the essential-states model for the conditions of Fig. 6. The times in part (a) are 5 a.u., 10 a.u., and 15 a.u. The spectrum at 40 a.u. is also shown in Fig. 6. In the long-time limit the peak heights are 53 and 26 a.u.

Figure 11 shows the time development of the kinetic-energy spectrum as calculated in the essential-states model for the situation in which the laser is tuned to the core resonant frequency. At shorter times the linewidths are limited by the pulse length, and are dependent on the laser turn on, but at longer times the linewidths are determined by the decaying states' lifetimes.

V. SUMMARY AND CONCLUSIONS

In this work, we have provided an extended essential-states description of the coherence-transfer effect predicted in Refs. [10] and [11], and we have compared the predictions of the essential-states model with exact numerical results for one-dimensional helium. We have found remarkably good agreement with the exact method, and thus infer that the essential-states model provides a suitable description of the coherence-transfer effect.

We conclude that when a neutral atom is photoionized, the kinetic-energy spectrum of out-coming electrons can be profoundly altered by tuning the photoionizing laser to an appropriate resonant frequency of the positive ion. In particular, a peak-splitting effect occurs. The peak splitting is consistent with what one would expect from a predressing of the final continuum states of the system, using the δ-function coupling (2).

We have shown that for a system in which the transition frequency to an autoionizing state is comparable to the transition frequency of the core resonance, one can superpose the coherence-transfer effect and laser-induced autoionization effects. Alternatively, for a system in which the frequencies are different, one can move from one effect to the other by adjusting the laser frequency, as discussed in [11].

In the present work, we have not sought to apply the analysis to any specific atoms. Nonetheless, the essential-states description applies in a three-dimensional real atom as well as to one-dimensional helium. Thus the effect should be experimentally verifiable, and experimental work motivated by Ref. [10] is now underway [20].

The coherence-transfer effect was first predicted in Ref. [10] within the context of photodetachment of negative ions. In Ref. [11] and in the present work, we have established that the effect applies in a more general context than photodetachment. We have worked within the context of ionization of a neutral atom, but it is clearly not limited to neutral initial states, but could be found in subsequent ionizations as well.

There are numerous variations on the system that could be considered and in which one would expect that the effect could still be seen. For example, one could use two lasers—one intense laser tuned to the core-resonance frequency to structure the final continua, and a second laser to drive transitions in the atom and to probe the final-state continua.

We have noted that in the pole approximation the core coupling does not affect the time development of the populations of the discrete states [21]. This result is quite different from that reported in studies of separable continuum-continuum couplings, since a separable continuum-continuum coupling changes the rate of decay from the discrete states [22]. Nonetheless, the δ-function coupling can affect the time development of the discrete states if one includes terms neglected in the pole approximation since the shifting of the thresholds of the continua causes the discrete states to "sample" slightly different energies in the continua. In our analysis we have assumed that the discrete-state–continuum matrix elements are independent of continuum energy, so it makes no difference which energy range is sampled. However, if the energy dependence of the matrix elements were included in the problem, then the shifting of the continua relative to the discrete states could influence the decay rates. This effect could be especially noticeable if a continuum resonance could be shifted into or out of the region "sampled."

We conclude with some general comments about the coherence-transfer effect. We stress that it differs from effects leading to the Knight doublet or to the asymmetric doublet of laser-induced autoionization because these other processes involve discrete-state–discrete-state couplings while the coherence-transfer effect involves a *continuum-continuum* coupling in which the *bound* electron changes state (e.g., $|1,E_k\rangle \rightarrow |2,E_k\rangle$). Also, it is explicitly a two-electron effect, while the usual Knight doublet requires only one electron. Of course, the LIA doublet also arises from a two-electron effect, and features transitions of the inner electron (e.g., $|1,2\rangle \rightarrow |2,2\rangle$), but the LIA doublet comes about from tuning to a resonant

frequency of the *preionized* system, not a resonant frequency of the final states. That is not to say that there is no middle ground between the two cases, however. In particular, Robicheaux [23] has examined a situation in which highly excited Rydberg states were coupled by transitions of the inner electron (e.g., $|1,n\rangle \rightarrow |2,n'\rangle$ for large n). If the Rydberg electron is barely bound, then the appropriate laser frequency for driving transitions of the inner electron approaches the resonant frequency of the positive ion.

Finally, we comment that the coherence-transfer phenomenon is related to laser-induced continuum structure effects [6]. The latter effects typically involve coupling a continuum to a discrete state, and also typically employ different lasers for photoionization than for structuring the continuum. The coherence-transfer effect as we have presented it, an the other hand, uses the same laser both to "prestructure" the final-state continua *and* to drive transitions within the ionizing system.

ACKNOWLEDGMENTS

We thank J. H. Eberly for his contributions. This work has been supported by Calvin College and by the National Science Foundation through Grant No. PHY-9408866 to Calvin College and Grant No. PHY-9111562 to the University of Rochester. R.G. acknowledges support by the Deutsche Forschungsgemeinschaft.

[1] P. L. Knight, Opt. Commun. **22**, 172 (1977); J. Phys. B **11**, L511 (1978).

[2] S. L. Autler and C. H. Townes, Phys. Rev. **100**, 703 (1955); P. L. Knight and P. W. Milonni, Phys. Rep. **66**, 21 (1980); P. L. Knight, M. A. Lauder, and B. J. Dalton, *ibid.* **190**, 1 (1991); W. Nicklich, H. Kumpfmüller, H. Walther, X. Tang, H. Xu, and P. Lambropoulos, Phys. Rev. Lett. **69**, 3455 (1992).

[3] L. Mower, Phys. Rev. **142**, 799 (1966); **165**, 145 (1968).

[4] For reviews of above-threshold ionization effects, see P. Agostini and G. Petite, Contemp. Phys. **29**, 57 (1988); J. H. Eberly, J. Javanainen, and K. Rzazewski, Phys. Rep. **204**, 331 (1991).

[5] Z. Deng and J. H. Eberly, Phys. Rev. Lett. **53**, 1810 (1984).

[6] P. L. Knight, Comments At. Mol. Phys. **15**, 193 (1984), reviews laser-induced continuum structure.

[7] U. Fano, Phys. Rev. **124**, 1866 (1961).

[8] See for example, P. Lambropoulos, Appl. Opt. **19**, 3926 (1980); P. Lambropoulos and P. Zoller, Phys. Rev. A **24**, 379 (1981); K. Rzazewski and J. H. Eberly, Phys. Rev. Lett. **47**, 408 (1981); Phys. Rev. A **28**, 3648 (1983). See also the review article of Ref. [2].

[9] G. S. Agarwal, S. L. Haan, K. Burnett, and J. Cooper, Phys. Rev. Lett. **48**, 1164 (1982). See also G. S. Agarwal, S. L. Haan, K. Burnett, and J. Cooper, *ibid.* **48**, 1164 (1982). See also G. S. Agarwal, S. L. Haan, and J. Cooper, Phys. Rev. A **29**, 2552 (1984); **29**, 2565 (1984), and references therein.

[10] R. Grobe and J. H. Eberly, Phys. Rev. A **48**, 623 (1993); J. H. Eberly and R. Grobe, in *Super-Intense Laser Physics,* Vol. 316 of *NATO Advanced Study Institute, Series B: Physics,* edited by B. Piraux, A. L'Huillier, and K. Rzazewski (Plenum, Amsterdam, 1993), p. 445; R. Grobe and J. H. Eberly, in *Multiphoton Processes,* Vol. 6 of *Series in Optics and Photonics,* edited by D. K. Evans and S. L. Chin (World Scientific, Singapore, 1994), p. 345.

[11] R. Grobe and S. L. Haan, J. Phys. B **27**, L735 (1994).

[12] Properties of the soft-core Coulombic potential $V(x)=-(1+x)^{1/2}$ are summarized in Q. Su and J. H. Eberly, Phys. Rev. A **44**, 5997 (1991). For previous two-electron applications see M. S. Pindzola, D. C. Griffin, and C. Bottcher, Phys. Rev. Lett. **66**, 2305 (1991); R. Grobe and J. H. Eberly, *ibid.* **68**, 2905 (1992); D. R. Schultz *et al.*, Phys. Rev. A **50**, 1348 (1994); and Refs. [13,14].

[13] R. Grobe and J. H. Eberly, Phys. Rev. A **48**, 4664 (1993).

[14] S. L. Haan, R. Grobe, and J. H. Eberly, Phys. Rev. A **50**, 378 (1994); in *Multiphoton Processes* [10], p. 365.

[15] A. I. Andryushin, M. V. Federov, and A. E. Kazakov, J. Phys. B **15**, 2851 (1982); A. I. Andryushin, A. E. Kazakov, and M. V. Federov, Zh. Eksp. Teor. Fiz. **82**, 91 (1982) [Sov. Phys. JETP **55**, 53 (1982)].

[16] J. Zakrzewski, J. Phys. B **17**, 719 (1984).

[17] See, for example, S. L. Haan and J. Cooper, Phys. Rev. A **28**, 3349 (1983).

[18] The computational techniques used are described in detail in Ref. [13].

[19] The resonance is broad enough that the Fano q parameter varies with energy across the resonance. The value -20 is a pole-approximation estimate.

[20] L. F. DiMauro (private communication).

[21] This result is discussed in, for example, P. R. Fontana, *Atomic Radiative Processes* (Academic, New York, 1982).

[22] L. Lefebvre and J. Beswick, Mol. Phys. **23**, 1223 (1972); L. Armstrong, Jr., C. E. Theodosiou, and M. J. Wall, Phys. Rev. A **18**, 2538 (1978); and Refs. [5,17].

[23] F. Robicheaux, Phys. Rev. A **47**, 1391 (1993).